Inorg. Chem. **2006**, *45*, 2750–2757

Characterization of Sol–Gel-Synthesized $LiFePO_4$ by Multiple Scattering XAFS

Marco Giorgetti* and Mario Berrettoni

Department of Physical and Inorganic Chemistry, University of Bologna and Unità di Ricerca INSTM di Bologna, Viale Risorgimento 4, 40136 Bologna, Italy

Silvera Scaccia and Stefano Passerini

ENEA (Italian Agency for New Technologies, Energy and the Environment), IDROCOMB, C.R. Casaccia, Via Anguillarese 301, 00060 Rome, Italy

Received December 12, 2005

X-ray absorption spectroscopy (XAS) was used to investigate the local structure arrangements of submicrocrystalline lithium iron phosphate and its precursors. The former material, proven to be very promising as active cathode material in lithium metal and lithium-ion batteries, was synthesized through a new procedure that combines a simple sol–gel precipitation with a moderate temperature (e.g., low cost) heat treatment. X-ray absorption near-edge structure (XANES) and extended X-ray absorption fine structure (EXAFS) spectra taken at the Fe K-edge pointed out the modification of the Fe site during the synthesis steps that allow one to produce the submicrometer size crystalline $LiFePO_4$ (active material) useful for batteries applications. The XAS investigation has shown that such a material is different from the conventional crystalline $LiFePO_4$ on the short-range order. The difference is attributed to the synthesis procedure.

Introduction

Lithium iron phosphate ($LiFePO_4$) has become of great interest as storage cathode for rechargeable lithium ion batteries because of its high energy density, low cost, and environmental benignancy and safety.[1] The material is a mixed ionic−electronic conductor in which the lithium ion diffusion and the poor electronic conductivity dominate the transport phenomenon. To increase the electrochemical performances of this material for use as storage cathode, a variety of material processing methods have been proposed by several researchers.[2−6] The results clearly show that both particle size reduction and intimate contact with a highly conductive material (usually carbon) improve the performance as a battery cathode of $LiFePO_4$ by reducing the solid-phase diffusion thickness for lithium ions and increasing the overall electronic conductivity for electron transport. In previous work[7,8] it was shown that submicrocrystalline $LiFePO_4$ produced by chemical lithiation of amorphous $FePO_4$ followed by a mild heating step is capable of delivering its full capacity when cycling at C/2 rate in liquid electrolytes. The performance of this material in discharge tests with nominal discharge times varying from 20 min to 10 h (the most useful range of battery discharge) is equal or superior to that of other $LiFePO_4$ material (doped or not doped) reported in the literature.[9]

The synthesis of the submicrocrystalline $LiFePO_4$ precursor material ($FePO_4$) has been extensively investigated

* To whom correspondence should be addressed. E-mail: marco.giorgetti@unibo.it. Phone: +39 051 209 3666. Fax: +39 051 209 3690.

(1) Padhi, A. K.; Nanjundaswamy, K. S.; Goodenough, J. B. *J. Electrochem. Soc.* **1997**, *144*, 1188.
(2) Yamada, A.; Chung, S. C.; Hinokuma, K. *J. Electrochem. Soc.* **2001**, *148*, A224.
(3) Yang, S.; Song, Y.; Ngala, K.; Zavalij, P. Y.; Whittingham, M. S. *J. Power Sources* **2003**, *119*−*121*, 239.
(4) Chung, S. Y.; Blocking, J. T.; Chiang, Y. M. *Nat. Mater.* **2002**, *1*, 123.
(5) Dominko, R.; Goupil, J. M.; Bele, M.; Gaberscek, M.; Remsar, M.; Hanzel, D.; Jamnik, J. *J. Electrochem. Soc.* **2005**, *152*, A858.
(6) Dominko, R.; Bele, M.; Gaberscek, M.; Remskar, M.; Hanzel, D.; Pejovnik, S.; Jamnik, J. *J. Electrochem. Soc.* **2005**, *152*, A607.
(7) Prosini, P. P.; Carewska, M.; Scaccia, S.; Wisniewski, P.; Passerini, S.; Pasquali, M. *J. Electrochem. Soc.* **2002**, *149*, A886.
(8) Prosini, P. P.; Carewska, M.; Scaccia, S.; Wisniewski, P.; Pasquali, M. *Electrochim. Acta* **2003**, *48*, 4205.
(9) Zane, D.; Carewska, M.; Scaccia, S.; Cardellini, F.; Prosini, P. P. *Electrochim. Acta* **2004**, *49*, 4259.

10.1021/ic0521170 CCC: $33.50
Published on Web 02/24/2006

previously.[10−12] In this work we focused on the structural characterization of the submicrocrystalline $LiFePO_4$ material and its precursors. The study was carried out using the X-ray absorption spectroscopy technique (XAS) as a local structural probe. The technique is sensitive to short-range order (a few angstroms around the selected atom) and can be applied to disordered, amorphous, crystalline,[13] and biological materials[14] and to solutions[15] as well. Previous reports based on XAS studies have given details on electrodes including electrochemical interfaces,[16] electrode surface,[17] and thermochromism.[18] Our group successfully applied the technique to the study of the local structure arrangements in V_2O_5-based cathode materials for lithium batteries.[19−26]

XAS studies on crystalline $LiFePO_4$ electrodes are also reported in the literature.[27,28] In these studies a special electrochemical cell[29] was used that allowed one to follow (in-situ) the lithium extraction/insertion process on a battery electrode. From the in-situ experiments, these researchers have concluded that a $LiFePO_4$ electrode in the discharged state (lithiated) contains Fe(II), whereas in the charged (delithiated) state ($FePO_4$) iron is found to be in the Fe(III) state. Also, they confirmed that the olivine structure of $LiFePO_4$ and $FePO_4$ was retained during repeated cycling.

In this report, we applied the XAS technique to study the structural and electronic modifications occurring in the Fe environment during the synthesis steps that produce the submicrocrystalline $LiFePO_4$ material, i.e., during the transformation of the pristine amorphous $FePO_4$ to lithiated amorphous $LiFePO_4$ and, finally, to crystalline $LiFePO_4$. The XAS data analysis has been conducted taking into account the multiple scattering (MS) formalism, which represents a better approach with respect to the one reported previously,[28] as demonstrated several times since the pioneering work on the MS formalism by Lee and Pendry[30] and further developed for the EXAFS case by the work of Natoli, Benfatto, and co-workers.[31,32] As a matter of the fact, our approach allowed us to obtain new physical insights into the structural characteristics of the investigated materials.

Table 1. List of the Investigated Compounds

sample a	sample b	sample c
amorphous $FePO_4$	amorphous $LiFePO_4$ (from lithiation of sample a)	crystalline LiFePO4 (from sample b, heated up to 550 °C)

Experimental Section

Synthesis and Samples Preparation. Amorphous iron(III) phosphate was synthesized by spontaneous precipitation from an equimolar aqueous solution of $Fe(NH_4)_2(SO_4)_2{\cdot}6H_2O$ and $NH_4H_2PO_4$ using hydrogen peroxide as the oxidizing agent. To a 0.025 M solution of $Fe(NH_4)_2(SO_4)_2{\cdot}6H_2O$ was added an equimolar solution of $NH_4H_2PO_4$, in the 1:1 volume ratio. Then, 3 mL of concentrated hydrogen peroxide solution was added to the solution at ambient temperature under vigorous stirring. A white precipitate started to form immediately after the addition of hydrogen peroxide. When the precipitation was completed, the precipitate was collected on a membrane filter (0.8 μm), washed several times with deionized water, and dried in oven at 400 °C for 24 h.

Amorphous $LiFePO_4$ was obtained by chemical lithiation of amorphous $FePO_4$ by using LiI as reducing agent. Amorphous $FePO_4$ was suspended in a 1 M solution of LiI in acetonitrile. The suspension was stirred for 24 h, filtered on a membrane filter (0.8 μm), washed several times with acetonitrile, and dried under vacuum. Crystalline $LiFePO_4$ was obtained by heating the latter (amorphous) compound in a tubular furnace at 550 °C for 1 h under reducing atmosphere (Ar/H_2 = 95/5). Table 1 summarizes the samples under investigation prepared following the above-mentioned procedures. X-ray powder diffraction of the investigated samples have been reported in previous publication[7,8] (see also Supporting Information), indicating an amorphous state for samples a and b and a transformation from amorphous to crystalline phase of the sample c, which the main peaks attributed to the olivine $LiFePO_4$ structure. The grain size of the crystallites, computed from the relevant diffraction peaks, quoted the crystallite dimensions to be between 85 and 100 nm.[8] Reference 7 also reports the SEM micrograph of the all investigated samples (see also Supporting Information) as well as the BET surface area.

Samples for the XAS experiments were mixed with boron nitride (90%) and then pressed as pellets (3 tons).

XAS Data Collection. X-ray absorption (XAS) experiments were performed at the Synchrotron Radiation Source (SRS) at Daresbury Laboratory, Warrington, England, using the beam line 7.1. The storage ring operates at 1.6 GeV and a typical current of 240 mA. A Si(111) double crystal was employed as a monochromator. To reduce higher harmonics, the second crystal was detuned around 70%. Internal references were used (Fe foil) for energy calibration

(10) Scaccia, S.; Carewska, M.; Di Bartolomeo, A.; Prosini, P. P.; *Thermochim. Acta* **2002**, *383*, 145.
(11) Scaccia, S.; Carewska, M.; Di Bartolomeo, A.; Prosini, P. P.; *Thermochim. Acta* **2003**, *397*, 135.
(12) Scaccia, S.; Carewska, M.; Prosini, P. P. *Thermochim. Acta* **2004**, *413*, 81.
(13) Filipponi, A. *J. Phys.: Condens. Matter* **2001**, *13*, R23.
(14) Giorgetti, M.; Ascone, I.; Berrettoni, M.; Conti, P.; Zamponi, S.; Marassi, R. *J. Biol. Inorg. Chem.* **2000**, *5*, 156.
(15) D'Angelo, P.; Benfatto, M.; Della Longa, S.; Pavel, N. V. *Phys. Rev. B* **2002**, *66*, 064209.
(16) Abruna, H. D. *Electrochemical Interfaces: Modern Techniques for In Situ Interface Characterization*; VCH: New York, 1991; pp 1−556.
(17) Tadjeddine, A.; Guay, D.; Ladouceur, M.; Tourillon, G. *Phys. Rev. Lett.* **1991**, *66*, 2335.
(18) Kulesza, P. J.; Malik, M. A.; Berrettoni, M.; Giorgetti, M.; Zamponi, S.; Schmidt, R.; Marassi, R. *J. Phys. Chem. B* **1998**, *102*, 1870.
(19) Giorgetti, M.; Passerini, S.; Smyrl, W. H.; Berrettoni, M. *Chem. Mater.* **1999**, *11*, 2257.
(20) Giorgetti, M.; Passerini, S.; Smyrl, W. H.; Berrettoni, M. *Inorg. Chem.* **2000**, *39*, 1514.
(21) Frabetti, E.; Deluga, G. A.; Smyrl, W. H.; Giorgetti, M.; Berrettoni, M. *J. Phys. Chem. B* **2004**, *108*, 3765.
(22) Giorgetti, M.; Mukerjee, S.; Passerini, S.; McBreen, J.; Smyrl, W. H. *J. Electrochem. Soc.* **2001**, *148*, A768.
(23) Giorgetti, M.; Passerini, S.; Smyrl, W. H.; Muckerjee, S.; Yang, X. Q.; McBreen, J. *J. Electrochem. Soc.* **1999**, *146*, 2387.
(24) Passerini, S.; Le, D. B.; Smyrl, W. H.; Berrettoni, M.; Tossici, R.; Marassi, R.; Giorgetti, M. *Solid State Ionics* **1997**, *104*, 195.
(25) Giorgetti, M.; Passerini, S.; Berrettoni, M.; Smyrl, W. H. *J. Synchrotron Radiat.* **1999**, *6*, 743.
(26) Giorgetti, M.; Berrettoni, M.; Passerini, S.; Smyrl, W. H. *Electrochim. Acta* **2002**, *47*, 3163.
(27) Haas, O.; Deb, A.; Cairns, E. J.; Wokaun, A. *J. Electrochem. Soc.* **2005**, *152*, A191.
(28) Deb, A.; Bergmann, U.; Cairns, E. J.; Cramer, S. P. *J. Phys. Chem. B* **2004**, *108*, 7046.
(29) Deb, A.; Bergmann, U.; Cairns, E. J.; Cramer, S. P. *J. Synchrotron Radiat.* **2004**, *11*, 497.
(30) Lee, P. A.; Pendry, J. B. *Phys. Rev. B* **1975**, *11*, 2795.
(31) Benfatto, M.; Natoli, C. R.; Bianconi, A.; Garcia, J.; Marcelli, A.; Fanfoni, M.; Davoli, I. *Phys. Rev. B* **1986**, *34*, 5774.
(32) Brouder, C.; Ruiz-Lòpez, M. F.; Pettifer, R. F.; Benfatto, M.; Natoli, C. R. *Phys. Rev. B* **1989**, *39*, 1488.

at each scan. This allows a continuous monitoring of the energy during consecutive scans. No energy drifts of the monochromator were observed during the experiments. Data were acquired in transmission mode. The ionization chamber was filled with an Ar/He gas mixture. XAS spectra were collected in the k space up to $k = 16$ Å^{-1} every 0.03 Å^{-1} with a five second integration time allowing EXAFS spectra to be recorded sequentially after the XANES region.

XAS Data Analysis. XANES spectra were normalized to an edge jump of unity taking into account the atomic background after the edge as it comes out from the EXAFS analysis. A prior removal of the background absorption was done by subtraction of a linear function extrapolated from the preedge region. The EXAFS analysis has been performed by using the GNXAS package[33,34] that takes into account the multiple scattering (MS) theory. The method is based on the decomposition of the EXAFS signals into a sum of several contributions, the n-body terms. The method allows the direct comparison of the raw experimental data with a model theoretical signal. The procedure avoids any filtering of the data and allows a statistical analysis of the results. The EXAFS signal was extracted using a set of polynomial spline (composed of two third-degree polynomials). The theoretical signal is calculated ab initio and contains the relevant two-body $\gamma^{(2)}$ and three-body $\gamma^{(3)}$ multiple scattering (MS) terms. The contribution from four-body $\gamma^{(4)}$ terms[35] has been checked out, but it was found negligible. The two-body terms are associated with pairs of atoms and probe their distances and variances. The three-body terms are associated with triplets of atoms and probe angles, bond−bond, and bond angle correlations. Data analysis is performed by minimizing a χ^2-like function that compares the theoretical model to the experimental signal.

The phase shifts for the photoabsorber and backscatterer atoms were calculated ab initio starting from the structural model available in the literature.[36] They were calculated according to the muffin-tin approximation. The Hedin−Lundqvist complex potential[37] was used for the exchange-correlation potential of the excited state. The core hole lifetime, Γ_c, was fixed to the tabulated value[38] and included in the phase shift calculation. The experimental resolution used in the fitting analysis was about 2 eV, in agreement with the stated value for the beamline used. The value of S_0^2 has been found to be between 0.78 and 0.91. The relevant E_0 values are found to be displaced of several eV with respect to the edge inflection point.

The EXAFS theoretical signals were calculated ab initio using the fractional atomic coordinates of crystalline $LiFePO_4$[36] available in the literature. This structural model was found suitable for the analysis of all samples, including the amorphous $FePO_4$, even though the crystalline $FePO_4$ is also known to have, besides the olivine structure,[36] a quartzlike form,[39] which is characterized by a tetravalent Fe site. Owing to the amorphous nature of sample a, and considering that the EXAFS parameters will be refined during the fitting procedure, there was no necessity of using two different starting model. In addition, when a deviation of more that 10% of a selected structural parameter (atomic distance, angle) occurred with respect to the crystallographic values, the corresponding theoretical signal was recalculated before being used in the fitting procedure.

The fitting procedure was conducted taking into account the relevant set of scattering path suggested by Haas et al.[27] with the implementation of the multiple scattering formalism, giving more reliability to the data analysis. Hence, we have included in the fitting procedures the following two-atom contributions: $\gamma_1^{(2)}$ Fe−O with degeneracy of 1; $\gamma_2^{(2)}$ Fe−O with degeneracy of 3; $\gamma_3^{(2)}$ Fe−O with degeneracy of 2; $\gamma_4^{(2)}$ Fe−P with degeneracy of 1; $\gamma_5^{(2)}$ Fe−O with degeneracy of 12; $\gamma_6^{(2)}$ Fe−Fe with degeneracy of 4. In addition, two three-body contributions, $\eta_1^{(3)}$ Fe−O−P and $\eta_2^{(3)}$ Fe−O−Fe, have been added as well, where $\eta_1^{(3)}$ Fe−O−P includes both $\gamma^{(2)}$ Fe--P and $\gamma^{(3)}$ Fe−O−P contributions and $\eta_2^{(3)}$ Fe−O−Fe includes both $\gamma^{(2)}$ Fe--Fe and $\gamma^{(3)}$ Fe−O−Fe contributions. It is worth pointing out that, due to the intrinsic asymmetry of the Fe octahedron, the different bond distances in the first Fe−O shell were taken into account considering three signals with different degeneracy. Also, the inclusion of the three-body term $\eta^{(3)}$ allowed one to monitor the shells beyond the second one by using the same three-atom coordinates both for the two-atom and the three-atom contributions. Hence, in our case, Fe—P and Fe—Fe interactions are probed in the same framework without the inclusion of new parameters. The overall number of parameters included in the fitting procedure was 24: 7 bond distances; 3 asymmetry coefficient β's; 2 angles; 9 EXAFS Debye−Waller factors; three nonstructural terms E_0, S_0^2, and the experimental resolution. It is worth mentioning that the number of fitting parameters does not exceed the estimated "number of independent data points" $N_{ind} = (2\delta k \delta R/\pi) + 2 = 36$, for $\delta k = 12.8$ and $\delta R = 4.5$. The independent data point to a number of parameters ratio that ensures the fit is overdetermined, pointing out the reliability of the minimization.

To evaluate the effect of the structural disorder, the simulation was performed by considering a non-Gaussian type of pair distribution functions. Because of the amorphous nature of the compound, in fact, a more flexible model replacing the simple Gaussian function is required. The Γ-like (Γ) distribution,[40,41] proven to be very useful in previous studied systems,[13,21,42] has been also used here. This function depends on three parameters: the average bond distance, the bond variance, and the asymmetry coefficient (skewness) β defined as K_3/σ^3, where K_3 is the third cumulant of the distribution. The full definition of the function is described in refs 13 and 41.

Results and Discussion

The XAS technique is particularly suitable for the study of the electronic and structural modification occurring during the multistep synthesis that produces the submicrocrystalline $LiFePO_4$ material due to the strong interaction between the photoejected electrons and the potential generated from the neighbors of the Fe center in the investigated materials. This study intends to figure out how and how far the local structure around the Fe center is altered by the chemical lithiation of amorphous $FePO_4$ and the successive heat treatment at medium temperature and to highlight the structural differences between the obtained submicrocrystalline material and the conventional one (available from the

(33) Filipponi, A.; Di Cicco, A.; Natoli, C. R. *Phys. Rev. B* **1995**, *52*, 15122.
(34) Filipponi, A.; Di Cicco, A. *Phys. Rev. B* **1995**, *52*, 15135.
(35) Giorgetti, M.; Berrettoni, M.; Filipponi, A.; Kulesza, P. J.; Marassi, R. *Chem. Phys. Lett.* **1997**, *275*, 108.
(36) Garcia-Moreno, O.; Alvarez-Vega, M.; Garcia-Alvarado, F.; Garcia-Jaca, J.; Gallardo-Amores, J. M.; Sanjuàn, M. L.; Amador, U. *Chem. Mater.* **2001**, *13*, 1570.
(37) Hedin, L.; Lundvquist, B. I. *J. Phys. C* **1971**, *4*, 2064.
(38) Krause, M.; Oliver, J. H. *J. Phys. Chem. Ref. Data* **1979**, *8*, 329.
(39) Mittal, R.; Chaplot, S. L.; Kolesnokov, A. I.; Loong, C. K.; Jayakumar, O. D.; Kulchreshtha, S. K. *Phys. Rev. B* **2002**, *66*, 174304.
(40) Filipponi, A. *J. Phys.: Condens. Matter* **1994**, *6*, 8415.
(41) Filipponi, A.; Di Cicco, A. *Task Q.* **2000**, *4*, 575.
(42) Dalba, G.; Fornasini, P.; Grisenti, R.; Rocca, F. *J. Non-Cryst. Solids* **2004**, *345&346*, 7.

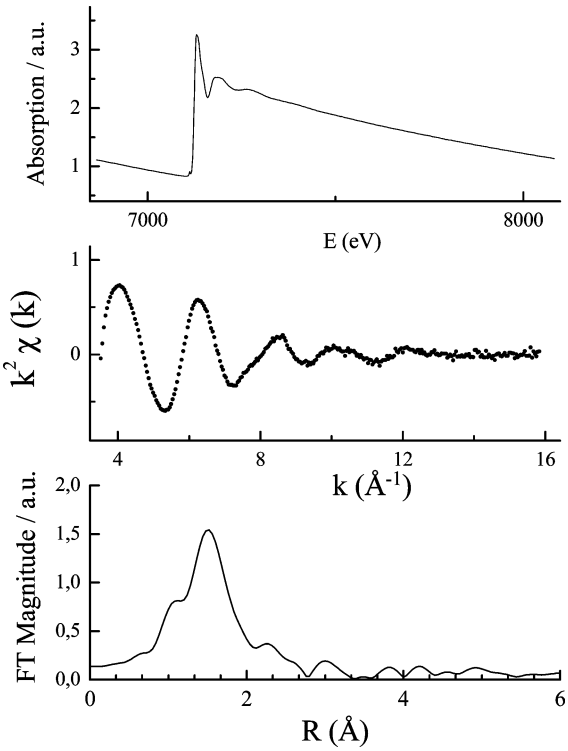

Figure 1. Preliminary data reduction of the Fe K-edge EXAFS spectrum of sample b. The upper panel shows the raw EXAFS spectrum, the k^2-extracted EXAFS is reported in the middle, and the relative Fourier transform of the k^2-extracted EXAFS is displayed at the bottom.

literature). XAS spectra were hence recorded at the Fe K-edge of the amorphous $FePO_4$ (sample a), amorphous $LiFePO_4$ (sample b, after chemical lithiation of sample a), and submicrocrystalline $LiFePO_4$ (sample c, after heating at 550 °C of sample b).

Figure 1, upper panel, shows a typical XAS absorption spectrum obtained at the Fe K-edge of the lithiated amorphous material (sample b). The spectrum includes the near-edge absorption region (XANES) extending to the first oscillation beyond the main edge and the extended X-ray absorption region (EXAFS) lasting up to the final point of the spectrum. The XANES region will be discussed first as it is often used as a qualitative probe of the chemical bonding and the oxidation state of the selected metal (Fe). The results of the EXAFS analysis, discussed later, will provide the local structure information as well as the estimation of the structural disorder around the Fe site. In Figure 1 is also shown a preliminary data reduction of the EXAFS spectrum: the k^2-extracted EXAFS signal is reported in the middle plot while the relative Fourier transform (FT) of the k^2-extracted EXAFS is displayed in the bottom panel. Figure 2 shows the k^2-extracted EXAFS signals of the all three samples investigated.

XANES. Figure 3 presents the XANES region of the XAS spectra obtained at the Fe K-edge of the compounds a−c. Since the curves are normalized (see the Experimental Section for details), it is allowed to directly compare the features shown by the three investigated materials. From the figure it is apparent that the XANES spectra differ both in the overall shape and in the energy position of the main peak,

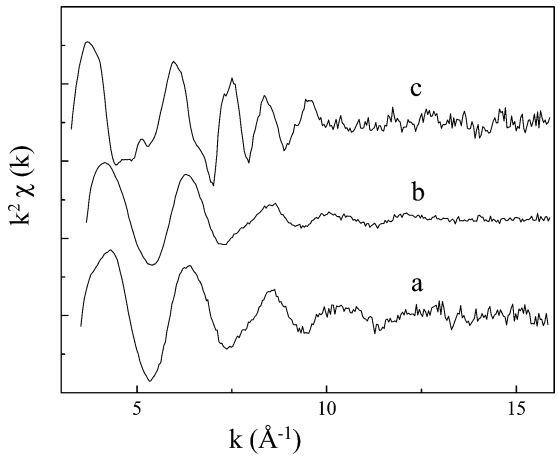

Figure 2. Experimental k^2-extracted EXAFS signals of the samples a−c obtained at the Fe K-edge.

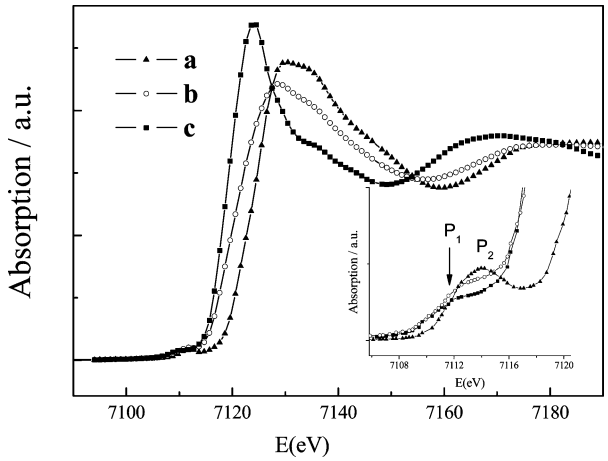

Figure 3. Experimental XANES spectra obtained at the Fe K-edge of the samples a−c. The curves are normalized as indicated in the Experimental Section. The inset shows a magnification of the preedge region.

thus providing information on both electronic and structural differences. Among the XANES features that are sensitive to the oxidation state of Fe only the preedge feature, which is due to the 1s−3d transition[27,28,43] and lies in the energy range between 7110 and 7115 eV, will be considered. In fact, although the edge and edge resonance regions (residing in the rising part and in the main absorption of the XANES spectrum at about 7115−7135 eV, respectively) also show a shift toward lower energy from sample a to c, the use of the preedge peak, as indicator[23] of the charge associated with the Fe, is preferred because it involves a transition to bound states. Besides, the edge resonance is associated with the continuum and involves multiple scattering resonances of the photoelectrons[44] and depends also on the interatomic distances and the coordination geometry.[45]

A magnification of the preedge region for the three samples is also presented in Figure 3. Sample a displays a preedge peak P_2 at an energy of about 7114 eV that moves toward lower values (P_1, at about 7112 eV) in the lithiated

(43) Cecchi, P.; Berrettoni, M.; Giorgetti, M.; Gioia Lobbia, G.; Calogero, S.; Stievano, L. *Inorg. Chim. Acta* **2001**, *318*, 67.
(44) Bunker, G.; Stern, E. A. *Phys. Rev. Lett.* **1984**, *52*, 1990.
(45) Clinton, D. E.; Tryk, D. A.; Bae, I. T.; Urbach, F. L.; Antonio, M. R.; Scherson, D. A. *J. Phys. Chem.* **1996**, *100*, 18511.

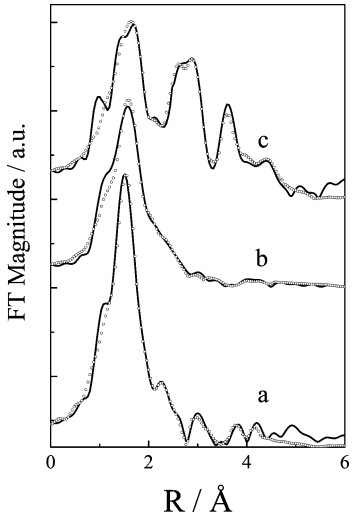

Figure 4. Experimental (—) and theoretical (▪▪▪) FT k^2-weighted EXAFS signals of the samples a−c obtained at the Fe K-edge. A Hanning window in the range $k = 3.5-15.9$ Å^{-1} was used.

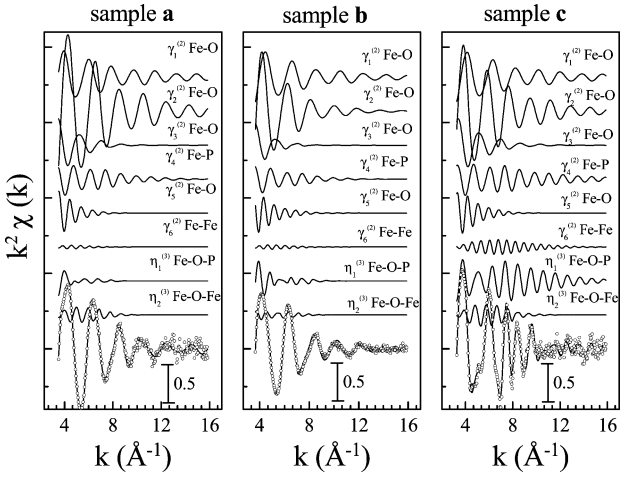

Figure 5. Details of the EXAFS analysis of the Fe K-edge of the samples a−c. The sample is indicated at the top of each panel. The figure shows the individual EXAFS contributions, in terms of two-body and three-body signals, to the total theoretical signal. At the bottom, the comparison of the total theoretical signal (—) with the experimental (▪▪▪) is also illustrated.

samples (b and c). On the basis of work available in the literature[27,46] the valence of Fe can be assumed +3 in the compound a and +2 in compounds b and c. Moreover, at the basis of this analysis, it is difficult to infer about the number of Fe^{3+} ions that go to the Fe^{2+}, even though the shift of the preedge peak is seen to be remarkable. The shift of the preedge peak also agrees with previous observations[27] performed on $LiFePO_4$ electrode material during charge/discharge test.

From the inset of Figure 3, a decrease of the preedge peak intensity is also observed. Preedge bands of iron(II) and iron (III) complexes were investigated extensively by Westre et al.,[47] and a full explanation of the preedge features is beyond the aim of the present work. Briefly, the occurrence of this peak is related to the nature of the 1s−3d transition, which is electric dipole forbidden but quadrupole allowed. Complexes in noncentrosymmetric environment have more intense preedge features than centrosymmetric complexes. The increase in intensity has been attributed to metal 4p mixing into 3d orbitals which provides some electric dipole allowed 1s−4p character to the transition and thus adds to the intensity from the quadrupole mechanism.[47]

From a structural viewpoint (considering that in this class of compounds Fe is in a octahedral environment) such a deviation from the centrosymmetric environment is likely to be observed just considering small variations of the FeO_6 octahedron, either Fe−O bond length or O−Fe−O angle variations. Our experimental findings imply that amorphous $FePO_4$ (sample a) is characterized by a more distorted FeO_6 octahedron than both the amorphous and crystalline lithiated materials ($LiFePO_4$, samples b and c).

EXAFS. Figure 4 shows a comparison of the FT signals obtained from the EXAFS spectra of the compounds under investigation, together with the theoretical curves obtained during the best fits procedure (see below). The curves have been obtained by preliminary analysis similar to that of Figure 1, using the same window of the corresponding k^2-EXAFS signals. The three curves appear different for both the intensity and the position of the peaks. The submicrocrystalline $LiFePO_4$ shows three main peaks at about 1.8, 2.8, and 3.6 Å. However, the first one is more intense in the unlithiated $FePO_4$ (sample a) than in the lithiated materials (samples b and c). The two other peaks at higher values are significantly visible only in sample c, whereas in samples a and b these peaks are present among others of low intensity.

From earlier considerations in the framework of a single scattering approach, the peak position of the FT curves is related to the radius of the backscattering shells of Fe, thus underlying that major modifications of the local atomic environment of Fe occur during the transformation of the amorphous compound (b) in the crystalline material (c). To obtain quantitative information on the local structure of Fe in the investigated compounds, we have fitted the experimental data with theoretical curves. The best-fit results are illustrated in Figure 5 panels a−c for the compounds a−c, respectively. Each panel of the figure shows the various contributions to the theoretical signal and the comparison of the theoretical signal with the experimental one. In the figure it is seen that the theoretical curves match well with the experimental ones in all panels, indicating the reliability of the chosen structural model and the accuracy of the data analysis. With reference to compound a, it is worth pointing out that some attempts to fit the experimental curve with a first shell formed by 4 oxygen describing an Fe tetrahedral site (quartzlike structure) were not succeeded. Figure 4 also compares the theoretical FT curves with the experimental ones, confirming the accuracy of the data analysis.

The interatomic distances and the corresponding EXAFS Debye−Waller factors of the samples investigated are shown in Table 2. The errors associated with the parameters

(46) Prince, A. A.; Mylswamy, S.; Chan, T. S.; Liu, R. S.; Hannoyer, B.; Jean, M.; Chen, C. H.; Huang, S. M.; Le, J. F.; Wang, G. X. *Solid State Commun.* **2004**, *132*, 455.
(47) Westre, T. A.; Kennepohl, P.; DeWitt, J. G.; Hedman, B.; Hogdson, K. O.; Solomon, E. I. *J. Am. Chem. Soc.* **1997**, *119*, 6297.

Table 2. Structural Parameters from EXAFS Fitting Results of Samples a−c with Estimated Parameter Errors Indicated in Parentheses[a]

MS signals	atomic dists/angles and corresponding variance	degeneracy	sample a	sample b	sample c
$\gamma_1^{(2)}$	Fe−O/Å	1	2.11(2)	1.996(5)	1.99(1)
	σ^2 Fe−O/Å^2		0.013(7)	0.004(1)	0.002(1)
$\gamma_2^{(2)}$	Fe−O/Å	3	1.976(4)	2.090(3)	2.114(6)
	σ^2 Fe−O/Å^2		0.008(2)	0.018(2)	0.003(1)
$\gamma_3^{(2)}$	Fe−O/Å	2	2.26(2)	2.31(3)	2.32(2)
	σ^2 Fe−O/Å^2		0.024(8)	0.033(4)	0.014(5)
$\gamma_4^{(2)}$	Fe−P/Å	1	2.84(2)	2.86(2)	2.86(1)
	σ^2 Fe−P/Å^2		0.008(4)	0.009(3)	0.003(2)
$\gamma_5^{(2)}$	Fe−O/Å	12	4.25(3)	4.32(3)	4.21(2)
	σ^2 Fe−O/Å^2		0.03(1)	0.03(1)	0.022(5)
$\eta_1^{(3)}$	O−P/Å	4	1.55(4)	1.50(3)	1.47(3)
	σ^2 O−P/Å^2		0.024(5)	0.009(4)	0.003(2)
$\gamma_6^{(2)}$	Fe−Fe/Å	2	4.85(3)	4.81(3)	4.70(1)
	σ^2 Fe−Fe/Å^2		0.03(1)	0.03(1)	0.010(6)
$\eta_1^{(3)}$	Fe−O−P/deg	4	141(2)	138(2)	132(2)
	σ^2 Fe−O−P/deg^2		39(12)	57(10)	21(8)
$\eta_2^{(3)}$	Fe−O−Fe/deg	4	122(3)	135(3)	121(2)
	σ^2 Fe−O−Fe/deg^2		20(10)	21(8)	15(8)
	Fe-P/Å	4	3.32[b]	3.34[b]	3.28[b]
	Fe−Fe/Å	4	3.78[b]	4.08[b]	3.86[b]

[a] The MS signals (path) correlated to the structural parameters are also indicated. [b] Data were obtained from geometrical consideration using the corresponding three-body atomic configuration.

obtained with the EXAFS analysis are indicated as well. The latter were determined by correlation maps (contour plots) for each pair of parameters. Figure 6 shows the contour plots for the Fe−O first shell and the E_0 variable for compound b, as an example. The estimated statistical error is associated with a 95% confidence interval.[48]

From the result of the fits reported in Figure 5 it is clear that all the signals included are important in determining the total theoretical signal. The main contribution to the first shell Fe−O is given by the second signal, $\gamma_2^{(2)}$ Fe−O, because of its higher degeneracy (3) with respect to $\gamma_1^{(2)}$ and $\gamma_3^{(2)}$. Indeed, the comparison of the three $\gamma_2^{(2)}$ Fe−O signals for the three materials reveals a lower amplitude of the oscillations in sample b with respect to that of samples a and c. This is also evidenced by the comparison of the corresponding EXAFS bond variance (listed in Table 2) that is a parameter related to the vibrational amplitude of the bond and takes into account both thermal and structural disorder. The same behavior is seen for the EXAFS bond variance of the $\gamma_3^{(2)}$ Fe−O signal. This fact is significant because the two signals take into account 5/6 of the Fe octahedron geometry. Though not always observed, the enhancement of the local disorder during ion insertion has been observed in several other intercalation materials, like spinel lithium manganese oxide,[49] $Li_xV_6O_{13}$,[50] and ZnV_2O_5.[19]

Another specific parameter related to the structural disorder is the asymmetric coefficient β for the $\gamma_2^{(2)}$ Fe−O first shell. As pointed out in the Experimental Section, to take into account the anharmonic effects of the first shell due to structural disorder, the Γ-like function was used, which leads to the Gaussian approximation when the asymmetric coefficient β approaches zero. From the fit outcome, it is seen that the asymmetric coefficient β is 0.5(2) in compound b, 0.2(1) in compound a, and almost zero in compound c. The increase of the vibrational amplitudes of the Fe−O first shell distance and the value of the asymmetric coefficient indicates a larger structural disorder present in sample b with respect to samples a and c. Therefore, these data indicate that the chemical lithiation induced an increase of the disorder in the local structure of the Fe environment. The nature of such disorder is structural, and it is due to the insertion of Li^+ ions in the $FePO_4$ structure. In the amorphous lithiated material (sample b) the Li^+ sites are not well established; however, the moderate heating step allows the Li^+ ions to move in the preferred sites to give a more ordered material (submicrocrystalline sample c**)**.

A close inspection of the Fe−O distances related to the first shell (taking into account the structural information obtained from the signals $\gamma_2^{(2)}$ Fe−O and $\gamma_3^{(2)}$ Fe−O) reveals the lengthening of the bonds while amorphous $FePO_4$ (sample a**)** is progressively transformed to submicrocrystalline $LiFePO_4$ (sample c**)**, with the main modifications occurring during the first step of the synthesis (from a to b), i.e., when iron is chemically reduced from Fe(III) to Fe(II). This behavior of the Fe−O interactions is found to be in agreement with literature results.[27] However, the Fe−O bond distances quoted for the crystalline sample c are different with respect to structural data on crystalline $LiFePO_4$[36,46,51] available in the literature.

Table 2 also indicated that the Fe−P interactions in the second and third shells are practically constant in all samples investigated. The inclusion of an Fe−O interaction at higher distance ($\gamma_5^{(2)}$ Fe−O) is justified from the high degeneracy of this path (12) that makes this signal contribute appreciably

(48) Filipponi, A. *J. Phys.: Condens. Matter* **1995**, *7*, 9343.
(49) Ammundsen, B.; Jones, D. J.; Roziere, J.; Burns, G. R. *Chem. Mater.* **1996**, *8*, 2799.
(50) Stallworth, P. E.; Kostov, S.; denBoer, M. L.; Greenbaum, S. G.; Lampe-Onnerud, C. *J. Appl. Phys.* **1998**, *83*, 1247.
(51) Yamada, A.; Chung, S. C.; Hinokuma, K. *J. Electrochem. Soc.* **2001**, *148*, A224.

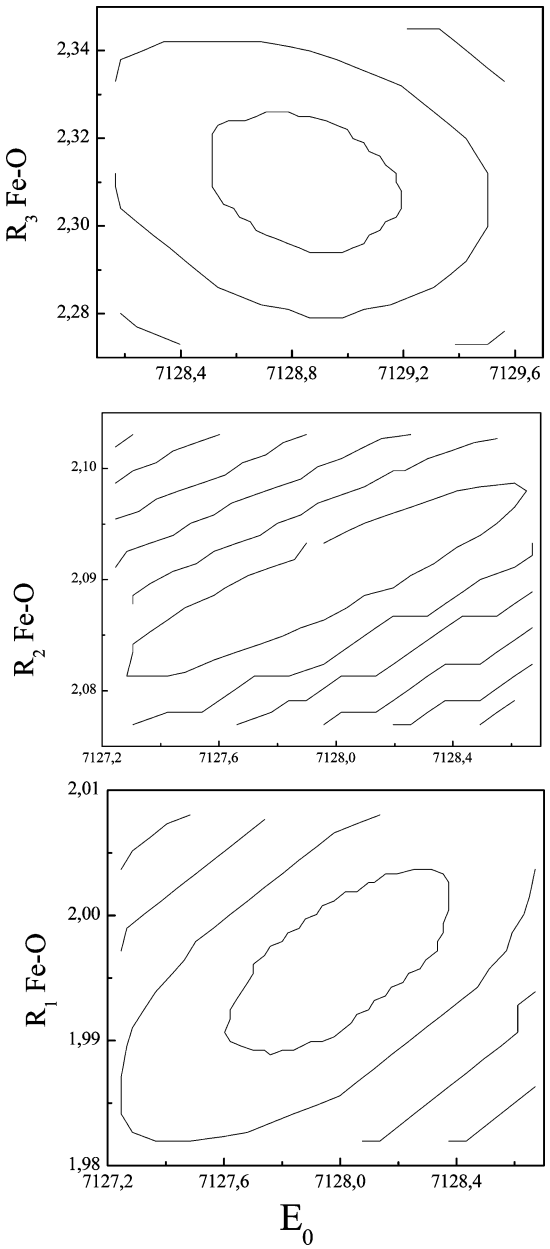

Figure 6. Two-dimensional section of the parameter space referring to the Fe−O first shell and E_0 (for sample b). Plots shows the three distance R_1 Fe−O, R_2 Fe−O, and R_3 Fe−O that correspond respectively to the signals $\gamma_1^{(2)}$ Fe−O, $\gamma_2^{(2)}$ Fe−O, and $\gamma_3^{(2)}$ Fe−O. The inner elliptical contour corresponds to the 95% confidence level.

at low k, in all samples. The Fe−Fe interactions were taken into account by means of the $\gamma_6^{(2)}$ signal and through the $\eta_2^{(3)}$ Fe−O−Fe one. The best-fit results indicate an expansion of the Fe−Fe interaction from 3.78 to 4.08 Å during the Li^+ accommodation into the amorphous network. This value decreased to the crystallographic one[36] upon the heating step (sample c) following the general trend observed for the Fe−O first-shell distances. The same behavior is observed for the Fe−Fe interaction at higher values, with two Fe atoms located at 4.70 Å from the photoabsorber in the crystalline sample c. These results indicate that the new synthesis approach of crystalline $LiFePO_4$ produces a material similar to the conventional one but with some differences detectable in the short-range order of the Fe site, as appear from the comparison of the structural parameters associated with the Fe first shell: sample c is seen to be characterized by two Fe−O at 2.32 Å, one Fe−O at 1.99 Å, and three Fe−O at 2.11 Å, whereas the conventional crystalline $LiFePO_4$[46,51] is characterized by by two Fe−O at 2.06 Å, two Fe−O at 2.25 Å, one Fe−O at 2.11 Å, and one Fe−O at 2.21 Å. On the contrary, the Fe−Fe interaction (long-range order) is quoted similarly (3.86 and 3.87 Å).

In Figure 5 it is also seen that the single MS signals of sample c are characterized by a higher intensity than the corresponding ones of samples a and b. This difference is especially observed for the interactions beyond the first shell. This experimental evidence is related to the long-range order of the compound investigated. The crystalline structure of sample c shows higher signal amplitudes because of the lower values of the corresponding damping factors, bond length, and angle variances. For example, it is worthwhile to notice the large signal contribution of the multiple scattering paths $\eta_1^{(3)}$ Fe−O−P and $\eta_2^{(3)}$ Fe−O−Fe. Such large contributions, which would have not been observed without the use of the MS formalism, show the importance of the inclusion of the MS formalism on the data analysis. For instance, due to the well-known limit of the single scattering approximation for the analysis of EXAFS spectra, previous data analyses on similar material[27,28] based on single-shell contributions (shells around the photoabsorber) were unable to select a fixed value of the coordination number of the Fe−Fe 3rd shell (2 or 4 in the refs 27 or 28). In this application, the Fe−Fe interaction has been probed by the $\eta_2^{(3)}$ Fe−O−Fe multiple scattering path, which allows one to monitor in the same framework without the inclusion of new parameters the Fe−O−Fe triplet (Fe−O distance and Fe−O−Fe angle) as well as the Fe−Fe distance, allowing the coordination number to converge to a well-fixed value (4).

Concluding Remarks

In this paper is reported the investigation of the structural and electronic properties of a submicrocrystalline iron phosphate material that has been proved promising as active cathode material in rechargeable lithium batteries. The study has involved the precursor amorphous $FePO_4$, the chemically lithiated precursor $LiFePO_4$, and the submicrocrystalline $LiFePO_4$ obtained by a moderate heating at 550 °C. The materials have been investigated by X-ray absorption spectroscopy, which allowed the investigation of amorphous and crystalline samples with the same experimental technique.

The results demonstrated that the submicrocrystalline iron phosphate material is characterized by a short-range order structure different from that of crystalline $LiFePO_4$ while no differences were detected in the long-range order. Also, Fe is reduced (mostly) from +3 to +2 during the chemical lithiation of the amorphous precursor and the local structure arrangement of Fe (octahedron) appears more distorted in the precursor than in the lithiated samples. Fe−O first-shell distances increase during the same step. In addition, data analysis evidenced an enhancement of the structural disorder during the lithiation of the amorphous precursor, which is

seen to vanish upon crystallization. In fact, Li^+ ions cause deformations on the local structure of the host ($FePO_4$ network). Afterward, upon heating, the structure becomes more organized with the Li^+ ions reaching the crystallographic sites.

To the best of our knowledge, this is the first time that the MS formalism has been used to analyze the XAS data in this class of compounds. In this respect, the inclusion of significant MS effects allowed us to upgrade the data analysis reported in a previous paper[27,28] by properly accounting for the structural contribution to the high-frequency component of the EXAFS spectrum.

Acknowledgment. Measurements at Daresbury Laboratory were supported by the European Community Research Infrastructure Action under the FP6 "Structuring the European Research Area" Program (through the Integrated Infrastructure Initiative "Integrating Activity on Synchrotron and Free Electron Laser Science").

Supporting Information Available: XRD and SEM data. This material is available free of charge via the Internet at http://pubs.acs.org.

IC0521170